



FXR overexpression alters adipose tissue architecture in mice and limits its storage capacity leading to metabolic derangements^S

Tim van Zutphen,^{1,2,*†} Johanna H. M. Stroeve,^{2,3,*} Jiufang Yang,* Vincent W. Bloks,* Angelika Jurdzinski,* Han Roelofsen,^{4,§} Nicolette C. A. Huijkman,* Theo H. van Dijk,*** Roel J. Vonk,[§] Jan van Deursen,^{††} Bart Staels,^{§§} Albert K. Groen,* and Folkert Kuipers^{1,****}

Departments of Pediatrics* and Laboratory Medicine,** and Center for Medical Biomics,[§] University Medical Center Groningen, University of Groningen, Groningen 9700 RB, The Netherlands; University of Groningen,[†] Campus Fryslân, Leeuwarden 8911 AE; The Netherlands; Department of Pediatrics and Adolescent Medicine,^{††} Mayo Clinic, Rochester, MN 55905; Univ. Lille,^{§§} INSERM, CHU Lille, Institut Pasteur de Lille, U1011-EGID, F-59000 Lille, France; and Amsterdam Diabetes Research Center and Department of Vascular Medicine,*** Academic Medical Center, Amsterdam 1105AZ, The Netherlands

Abstract The bile acid-activated nuclear receptor, FXR (NR1H4), has been implicated in the control of lipid and energy metabolism, but its role in fat tissue, where it is moderately expressed, is not understood. In view of the recent development of FXR-targeting therapeutics for treatment of human metabolic diseases, understanding the tissue-specific actions of FXR is essential. Transgenic mice expressing human FXR in adipose tissue (aP2-hFXR mice) at three to five times higher levels than endogenous *Fxr*, i.e., much lower than its expression in liver and intestine, have markedly enlarged adipocytes and show extensive extracellular matrix remodeling. Ageing and exposure to obesogenic conditions revealed a strongly limited capacity for adipose expansion and development of fibrosis in adipose tissues of aP2-hFXR transgenic mice. This was associated with impaired lipid storage capacity, leading to elevated plasma free fatty acids and ectopic fat deposition in liver and muscle as well as whole-body insulin resistance.^{¶¶} These studies establish that adipose FXR is a determinant of adipose tissue architecture and contributes to whole-body lipid homeostasis.—van Zutphen, T., J. H. M. Stroeve, J. Yang, V. W. Bloks, A. Jurdzinski, H. Roelofsen, N. C. A. Huijkman, T. H. van Dijk, R. J. Vonk, J. van Deursen, B. Staels, A. K. Groen, and F. Kuipers. **FXR overexpression alters adipose tissue architecture in mice and limits its storage capacity leading to metabolic derangements.** *J. Lipid Res.* 2019. 60: 1547–1561.

Supplementary key words farnesoid X receptor • hypertrophy • hyperplasia • extracellular matrix • insulin resistance

Bile acids are amphipathic steroids made from cholesterol in the liver that act as facilitators of intestinal fat absorption (1). It has become clear that this versatile group of molecules also regulates an array of physiological processes that are vital to hepatic, intestinal, and metabolic health via activation of the nuclear receptor, FXR (NR1H4), and the membrane-bound receptor, TGR5 (GPBAR1) (1, 2). Bile acids have also been shown to be able to activate the nuclear receptors, vitamin D receptor and pregnane X receptor, as well as sphingosine 1-phosphate receptor 2 (3–5). The combined properties of being small molecules with potent physiological effects have driven efforts to utilize bile acids and/or their signaling systems for therapeutic applications (2). Obeticholic acid, a potent FXR agonist, has been approved for the treatment of primary biliary cholangitis (6). Obeticholic acid was also shown to increase insulin sensitivity in type 2 diabetes patients as well as to

Abbreviations: aP2-hFXR mice, transgenic mice expressing human FXR in adipose tissue; *Cd68*, cluster of differentiation 68; ECM, extracellular matrix; eWAT, epididymal white adipose tissue; GSEA, Gene Set Enrichment Analysis; HFD, high-fat diet; iWAT, inguinal white adipose tissue; *Mcp1*, monocyte chemoattractant protein 1; rWAT, retroperitoneal white adipose tissue; *Shp*, small heterodimer partner; WAT, white adipose tissue.

The data discussed in this publication have been deposited in NCBI's Gene Expression Omnibus (van Zutphen et al., 2019) and are accessible through GEO Series accession number GSE37248 (<http://www.ncbi.nlm.nih.gov/geo/query/acc.cgi?acc=GSE37248>).

¹To whom correspondence should be addressed.

e-mail: t.van.zutphen@umcg.nl (T.v.Z.); f.kuipers@umcg.nl (F.K.)

²T. van Zutphen and J. H. M. Stroeve contributed equally to this work.

³Present address of J. H. M. Stroeve: Food and Biobased Research, Bornse Weiland 9, 6708 WG Wageningen, The Netherlands.

⁴Present address of H. Roelofsen: van Hall Larenstein, Agora 1, 8934 CJ Leeuwarden, The Netherlands.

^SThe online version of this article (available at <http://www.jlr.org>) contains a supplement.

This work was supported by CardioVascular Onderzoek Nederland Grant CVON 2018-27 (F.K., A.K.G.) and the Noaber Foundation (F.K.). The authors have no competing interests to declare.

Manuscript received 3 April 2019 and in revised form 24 June 2019.

Published, JLR Papers in Press, June 28, 2019

DOI <https://doi.org/10.1194/jlr.M094508>

Copyright © 2019 van Zutphen et al. Published under exclusive license by The American Society for Biochemistry and Molecular Biology, Inc.

This article is available online at <http://www.jlr.org>

improve markers of liver inflammation and fibrosis (7). Effectiveness of obeticholic acid treatment was also confirmed in a multicenter trial with noncirrhotic nonalcoholic steatohepatitis patients (8). Interestingly, despite hepatic improvements, this study also showed elevated insulin levels and increased values for the homeostatic model assessment of insulin resistance index. Yet, the many implications of bile acid signaling pathways on energy metabolism have inspired the development of FXR agonists aiming at obesity-related diseases that are currently advancing into clinical trials (9–12).

FXR activation by bile acids (13–15) provides these natural detergents with a means to modulate their own synthesis in the liver and their transport within the enterohepatic circulation (1, 16–18). Accordingly, FXR shows highest expression in the liver and intestine (19). Yet, *FXR* expression is not confined to these sites, but also occurs in several other organs and tissues, including kidney, adrenal glands, and vascular wall as well as adipose tissue. The physiological functions of FXR at these locations have largely remained elusive. In view of the recent developments toward the use of FXR agonists as therapeutic agents, it is of crucial importance to have full understanding of the (patho)physiological role of FXR in specific non-enterohepatic locations, including adipose tissue. This is of particular importance because obesity-associated diseases, such as type 2 diabetes and dyslipidemia, are characterized by adipose tissue dysfunction (20).

The capacity for dynamic remodeling of white adipose tissue (WAT) and its role in control of whole-body metabolism through cross-talk with other tissues and organs by metabolites (predominantly free fatty acids) and hormones (i.e., adipokines and lipokines) delineate the complexity of metabolic control (21). Whereas subcutaneous WAT is the sole site in the body that can accumulate lipids without detrimental consequences, expansion of visceral adipose depots and, particularly, ectopic lipid deposition in liver and muscle have major adverse health effects (22). Expansion by formation of new adipocytes (hyperplasia) is a hallmark of healthy WAT, whereas growth by enlargement of adipocyte size (i.e., hypertrophy) is associated with adverse metabolic outcomes (23).

A role for FXR in adipose tissue, where it is expressed at relatively low levels, was first proposed when *FXR*^{−/−} mice were shown to exhibit small adipocytes, and FXR was subsequently shown to promote adipocyte differentiation in vitro (24–26). These initial studies further revealed insulin resistance in adipose tissue of mice lacking *Fxr*. Unexpectedly, whole-body FXR-deficient mice were also shown to be resistant to the development of obesity when fed a high-fat diet (HFD) or after crossbreeding with a genetic model of obesity, i.e., *ob/ob* mice. Both models showed improved glucose homeostasis as well as increased adipose insulin sensitivity (27). Interestingly, *Fxr* expression in adipose tissues appeared to be decreased in mouse models of obesity (24). Yet, the direct contribution of adipocytic FXR in the development of these striking metabolic phenotypes has remained elusive.

Here, we describe the metabolic consequences of moderate (3- to 5-fold) overexpression of human *FXR* under

the control of the aP2 (*Fabp4*) promoter in mice to directly address FXR function in adipose tissue. These studies show that, in line with the small adipocytes observed in *FXR*^{−/−} mice (24), transgenic mice expressing human *FXR* in adipose tissue (aP2-hFXR mice) display a marked adipocyte hypertrophy. We examined the impact of FXR overexpression on WAT functioning under basal conditions as well as in response to metabolic stressors, such as diet- and age-induced obesity. These studies establish that FXR is a key determinant of adipocyte size and fat tissue architecture, as sustained *FXR* expression in adipose tissue limits its storage capacity, promotes adipose tissue fibrosis, and ultimately drives ectopic lipid accumulation and development of whole-body insulin resistance.

MATERIAL AND METHODS

Transgene construction and generation of transgenic aP2-hFXR mice

The individual expression plasmids containing the mouse aP2 promoter in pBleuscript II SK(+) and the full-length open reading frame of the human *FXRα2* in pCDNA3.1/TOPO were generous gifts from Dr. R. E. Hammer (28) and Dr. R. Mukherjee (29), respectively.

The 5.4 kbp fragment of aP2 promoter was excised from the pBleuscript II SK(+) using KpnI-SmaI restriction enzymes and ligated into the *KpnI* and *SmaI* sites of the pGEM-7Zf(+) vector (Promega, Madison, WI). By PCR amplification, *SmaI*-*SmaI* restriction sites were cloned onto the human *FXRα2* fragment (using forward primer cccgggATGGGATCAAAAATGAATCT and reverse primer cccgggAGAATAGAATGACACCTACT). The resulting 1.9 kbp *SmaI*-*SmaI* human *FXRα2* fragment was cloned into the pCRTMII vector (Invitrogen, Breda, The Netherlands). After amplification, this fragment was excised, gel purified, and ligated to *SmaI*-*SmaI* sites of the pGEM-7Zf(+) containing the 5.4 kbp aP2 promoter fragment. The orientation of the human *FXR* gene was verified using gel-based restriction control and the plasmid was sequence verified for the presence of the correct fragment. Adipocyte-specific human-FXR transgenic mice (aP2-hFXR mice) were generated by microinjection of the construct in fertilized FVB/NHsd eggs. The clone with the highest human-*FXR* mRNA level was recovered. Wild-type littermates were used as a control. aP2-hFXR mice were mated with whole-body *Fxr*-deficient (*FXR*^{−/−}) mice in two steps, generating progeny including *FXR*^{−/−} and aP2-hFXR mice on a *FXR*^{−/−} background. Male mice used in this study were housed in a light (12:12 h)- and temperature (21°C)-controlled facility and received laboratory chow (RMH-B) and water ad libitum. When indicated, mice were fed a HFD containing 60% calories from fat, composed of 36% (w/w) beef fat (diets were obtained from Abdiets, Woerden, The Netherlands). Fat and lean mass was determined by MRI (Minispec, LF 90 II; Brüker, Billerica, MA). Four hour-fasted animals were euthanized under anesthesia, and organs and tissues were carefully dissected and weighed. All experimental procedures were approved by the review board of the Animal Care and Use Committee of the Groningen University in accordance with local regulations for use of experimental animals.

Histology and adipocyte size determination

The samples from liver and WAT fat depots were fixed in 4% neutral buffered paraformaldehyde, embedded in paraffin, cut into 4 μm sections, and stained with either H&E or picrosirius red

staining by standard procedures. Cell area of three times sixty adipocytes per animal ($n = 6-8$ per group) was quantified using image analysis software (Qwin; Leica, Wetzlar, Germany). Crown-like structure abundance was determined in H&E-stained sections by counting CLS prevalence per square millimeter in whole sections of at least 10 mm².

Indirect calorimetry

Mice were placed in an open-circuit indirect calorimeter system 24 h prior to the start of the experiment with free access to water and food (TSE Systems GmbH, Bad Homburg, Germany). Flow rates were measured and controlled with a mass flow controller. O₂ and CO₂ concentrations of dried inlet and outlet air from each chamber were measured every 10 min. Infrared light-beam frames surrounding the home cage measured activity in the x and y direction. Data were analyzed using LabMaster software (TSE Systems GmbH). Energy expenditure was calculated using the following equation: EE (kcal/h) = $[3.941 \times \text{VO}_2 \text{ (ml/h)} + 1.106 \times \text{VCO}_2 \text{ (ml/h)}]/1,000$.

Fat absorption

Fat absorption was determined as described previously (30).

Hepatic de novo lipogenesis

Labeling of the acetyl-CoA pool was assessed by providing [$1\text{-}^{13}\text{C}$]acetate (Isotec/Sigma-Aldrich, St. Louis, MO) in drinking water as previously described by Jung et al. (31). Lipids in liver homogenates were fractionated using Isolute NH₂ columns (Biotage AB, Uppsala, Sweden) and subsequently converted to their pentafluorobenzyl derivatives.

GC-MS measurements of fatty acids and calculations of de novo lipogenesis and chain elongation of fatty acids were performed essentially as described (32). Pre-existing fatty acids (percent) were calculated by the following equation: $100\% - \text{de novo synthesis (\%)} - \text{chain elongation (\%)} = \text{originating fatty acids}$.

Real-time quantitative reverse transcription-PCR

Total RNA was isolated from tissues using TRIreagent (Sigma-Aldrich). cDNA was synthesized by reverse transcription using reverse transcriptase and random primers according to the manufacturer's protocol. mRNA expression levels were analyzed by means of real-time PCR on a 7900HT FAST real-time PCR system using FAST PCR master mix and MicroAmp FAST optical 96-well reaction plates (Applied Biosystems Europe, Nieuwerkerk a/d IJssel, The Netherlands) using SYBR green and $\Delta\Delta\text{CT}$ for all genes except *Fxr* that could only be detected using TaqMan. PCR results were normalized to 36b4 (*Rplp0*) mRNA levels. Primers and probe sequences are listed in Table 1.

Liver and plasma parameters

Hepatic lipids were extracted from homogenized livers in ice-cold PBS; lipids were extracted according to Bligh and Dyer (33). Lipid profiles in liver and plasma were determined using commercially available kits for free fatty acids, triglycerides, and cholesterol (Wako, Neuss, Germany; Roche, Mannheim, Germany). Blood glucose and insulin concentrations were measured using a EuroFlash meter (Lifescan Benelux, Beerse, Belgium) and an ELISA (Mercodia, Uppsala, Sweden), respectively. For analysis of glucose kinetics, a trace amount of labeled 13-C glucose was injected intraperitoneally into 9 h-fasted mice and total glucose was measured every 10 min and blood spots were collected. Glucose kinetics were determined according to (34). Adipokine array was performed according to the manufacturer's instructions (R&D Systems, Minneapolis, MN), using 50 μl of pooled plasma from six animals per group.

Plasma bile acids

Bile acid concentration in plasma was measured in 25 μl of homogenized plasma. An internal standard containing D4-choleate, D4-chenodeoxycholate, D4-glycocholate, D4-taurocholate, D4-glycochenodeoxycholate, and D4-taurochenodeoxycholate was added. Samples were mixed and centrifuged at 15,900 g. The supernatant was evaporated under vacuum at 40°C and reconstituted in 100 μl of 50% methanol. The bile acid profile was measured using LC-MS/MS as described (35).

Affymetrix microarray analysis

For the microarray analysis, total RNA was prepared from epididymal WAT (eWAT) of 10-week-old wild-type and aP2-hFXR-TG mice ($n = 4$ per group) using TRIreagent (Sigma-Aldrich). RNA was further purified using RNeasy MinElute micro columns (Qiagen, Venlo, The Netherlands). RNA integrity was checked on an Agilent 2100 bioanalyzer (Agilent Technologies, Amsterdam, The Netherlands) using 6000 Nano Chips according to the manufacturer's instructions. Five hundred nanograms of RNA were used for one cycle cRNA synthesis (Affymetrix, Santa Clara, CA). Hybridization, washing, and scanning of Affymetrix Gene Chip Mouse Gene 1.0 ST arrays were done according to standard Affymetrix protocols. Quality control, normalization (VSN), pre-filtering (fold change 1.1), and statistics (IBMT) were performed in MADMAX (36). A list of significantly changed annotated genes, including FDR-corrected *P*-values (5%) was generated. All microarray data reported are described in accordance with MIAME guidelines and are available in the GEO database (GSE37248). Identification of overrepresented functional categories among responsive genes and their grouping into functionally related clusters was performed using DAVID 6.7 functional annotation clustering tool (37) and Gene Set Enrichment Analysis (GSEA) (38). Transcription factor analysis was performed with Metacore, Clarivate Analytics.

Adipose tissue culture and CILAIR

At 14 weeks of age, wild-type ($n = 6$) and aP2-hFXR ($n = 5$) mice were euthanized. eWAT was flushed with saline solution to remove blood from the tissue and carefully dissected. The adipose tissue culture protocol is described (39). The CILAIR protocol was described previously (40). Briefly, after mincing (20–80 mg pieces), washing, filtering, and centrifuging the adipose tissue, the tissue was weighed and tissue pieces of individual wild-type and aP2-hFXR mice were pooled and divided over three wild-type dishes (1.2 g per dish in 12 ml of medium) and three aP2-hFXR-TG dishes (0.75 g per dish in 7.5 ml of medium). Dishes with adipose tissue were incubated at 37°C at 5% CO₂ with lysine and arginine-free DMEM medium (D944; Sigma-Aldrich) supplemented with 50 $\mu\text{g}/\text{ml}$ gentamicin (15750; Invitrogen), 100 mg/l leucine-HCl (L8912; Sigma-Aldrich), and 200 mg/l proline (P5607; Sigma-Aldrich) to deplete the ¹²C lysine and arginine pool in the tissue. The medium was renewed after 1, 16, 20, and 23.5 h. After the last wash, all six dishes received fresh DMEM medium containing 100 mg/l L-[¹³C₆, ¹⁴N₂]lysine and 100 mg/l [¹³C₆, ¹⁵N₄]arginine (Cambridge Isotope Laboratories, Andover, CT). Tissues were maintained in culture for an additional 24 h to allow incorporation of the label into newly synthesized proteins. Thereafter, media were collected and stored at -80°C until analysis. After concentration of the culture media to a final volume of approximately 30 μl by ultrafiltration, medium samples were fractionated by SDS-PAGE on 4–12% bis-Tris gel with a MOPS buffer (NuPAGE®-Novex; Invitrogen). Bands were visualized and whole lanes were excised into 25 pieces that were processed for tryptic digestion. Each gel piece was washed, in-gel reduced, washed, and rehydrated for 20 min by adding 5 ng/ μl of modified trypsin

TABLE 1. Primers used in the study

Gene	Forward	Reverse
<i>36B4 (Rplp0)</i>	CTGTTGGCCAATAAGGTGCC	GGAGGTCTTCTCGGGTCTCTA
<i>Abca1</i>	CCCAGAGCAAAAAGCGACTC	GGTCATCATCACTTTGGTCCTTG
<i>Abcg1</i>	CAAGACCCCTTTTGAAGGGATCTC	GCCAGAATATTCATGAGTGTGGAC
<i>Bgn</i>	CCTCCCCAGGAACATTGACC	CAAGGTGAGTAGCCACAGGG
<i>Ccr7</i>	ACCCAGGGAAACCCAGGAAA	GGCAGAAGCACACCTGGAAA
<i>Cd68</i>	CACCTTCGGGGCATGTTTCTC	AGGACCAGGCCAATGTAGAG
<i>Col1a1</i>	CGGCTCCTGCTCCTCTTAGG	CTGACTTCAGGGATGTCTTCTTGG
<i>Col1a2</i>	TGTGGATACGCGGACTCTGTT	CTGATCCCGATTGCCAAATATTGG
<i>Col6a1</i>	TGCCACAGACCACACATACC	TTTCCTCGCTCCCCCTCATA
<i>Fxr</i>	CTCCTGGGTGCGCTGAC	GACATCAGCATCTCAGCGTG
		Probe: CGGACATTCAATCATCAC
<i>Il-10</i>	TGCAGGACTTTAAGGGTTACTTGG	CAGGGAATTCAAATGCTCCTTG
<i>Leptin</i>	AAGACCATTGTCACCAGGATCAA	GTTCCATCTTGGACAACTCAGA
<i>Mcp1</i>	GGCTCAGCCAGATGCAGTTAA	AGCCTACTCATTGGGATCATCTT
<i>Mgl1</i>	AACCCAAGAGCCTGGTAAAGC	CGGAGACGACCACCAACA
<i>Mgl2</i>	ATGGAGTCTCCAAAGTTTGCTCTAA	TCACGGAGATGACCACCAGTA
<i>Sr-b1</i>	TCAGAAGCTGTTCTTGGTCTGAAC	GTTTCATGGGGATCCCAGTGA
<i>Tnfa</i>	GTAGCCACGTCGTAGCAAAC	AGTTGGTTGTCTTTGAGATCCATG

(Promega) in 20 mM ammonium bicarbonate. Digestion was carried out overnight at 37°C. After digestion, the peptides were extracted from the gel by drying the gel pieces by speed-vac, rehydrating with 0.1% trifluoroacetic acid, and dehydrating with 0.1% trifluoroacetic acid in 100% ACN. The extracted peptides were dried by speed-vac and redissolved in a MS-compatible solvent (0.1% formic acid). Separation of the resulting tryptic peptide mixtures was performed by nanoscale reversed-phase LC-MS/MS. Protein identification and data analyses were performed as described (32).

Minor adjustments made to this protocol were: 1) Selected mass range of m/z 300–1,100 in Analyst QS 1.1 software (Applied Biosystems, Carlsbad, CA). 2) Selected three abundant charged peptides were dynamically excluded for 90 s with 50 mmu mass tolerance. 3) ProteinPilot 3.0 software (Applied Biosystems) using the UniprotKB/Swiss-Prot database was used to generate peak lists. Chosen options within the program were: label, Lys+6, and Arg+10; Cys alkylation with iodoacetamide; trypsin digestion; gel-based identification; species, *Mus musculus*; identification focus for biological modifications; thorough search.

Western blot

Tissue lysates were prepared in RIPA lysis buffer [Tris-HCl (pH 8), NaCl 138 mM, NP40 1%, KCL 2.7 mM, MgCl₂ 1 mM, glycerol 5%, EDTA 5 mM, Na₃VO₄ 1 mM, NaF 20 mM, DTT 1 mM, and protease inhibitor] and protein concentrations were quantified using the RC DC assay (Bio-Rad, Hercules, CA). Protein samples were subjected to SDS-PAGE (15% gels) and transferred to nitrocellulose using a Trans-Blot® Turbo™ transfer system (Bio-Rad). Membranes were blocked for 1 h at room temperature in PBS containing 0.1% Tween and 2% milk powder and incubated for 16 h with primary antibodies at 4°C. Antibodies used in this study were: anti-lamin A/C (Cell Signaling), anti-Col-1 (Southern Biotech, Birmingham, AL), and anti-GAPDH (Calbiochem, San Diego, CA). Proteins were detected by incubating the blot with HRP-conjugated donkey anti-rabbit (Life Science; NA934) or HRP-conjugated rabbit anti-mouse (Dako; p0260) IgG for 1 h at room temperature. Bands were visualized using Supersignal West Dura substrate (Thermo Scientific, Waltham, MA) and ChemiDoc (Bio-Rad). Image Lab software (Bio-Rad) was used for densitometry.

Statistical analysis

Data are presented as mean ± SEM. Differences between groups were tested by nonparametric Mann-Whitney U-test using

GraphPad Prism 5.00 software package (GraphPad Software, San Diego, CA). All values are given as mean ± SEM. Significance was indicated as * P < 0.05, ** P < 0.01, and *** P < 0.001.

RESULTS

aP2-hFXR mice have reduced body weight and enlarged adipocytes

To explore the role of FXR in adipose tissue, we generated transgenic mice that overexpress *FXR* (NR1H4) under control of the aP2 (*Fabp4*) promoter. Specifically, a transgenic construct containing the mouse aP2 promoter region and the human *FXR* coding sequence was microinjected into fertilized mouse eggs (supplemental Fig. S1A). Transgenic founders were produced and characterization of two independent transgenic lines, expressing the highest levels of total *FXR* mRNA in fat tissues, revealed highly similar phenotypes. In the transgenic line used for these experiments (designated aP2-hFXR), the total *FXR* mRNA expression level was increased 5.8-, 3.1-, and 3.2-fold in eWAT, retroperitoneal WAT (rWAT), and subcutaneous inguinal WAT (iWAT), respectively, but expression was still modest when compared with expression of endogenous *Fxr* in liver and ileum (Fig. 1A).

Body weights of 14-week-old male transgenic mice were ~20–30% lower than those of control mice (Fig. 1B). Food intake was slightly reduced in aP2-hFXR mice (Fig. 1C). The decrease in body weight is unlikely due to reduced intestinal absorption efficiency, as dietary fat absorption was unaffected (supplemental Fig. S1B). A small but significant difference between aP2-hFXR mice and controls was observed in locomotor activity during the light phase (Fig. 1D). As the effects of the absence of *Fxr* in whole-body *FXR*^{−/−} mice on carbohydrate metabolism were most apparent during fasting and refeeding (41, 42), indirect calorimetry was performed during fed, fasted, and refeed conditions. Energy expenditure did not significantly differ between both groups under these conditions, and also not during fasting and refeed conditions (Fig. 1E, supplemental Fig. S1C). Growth curves showed that the body weight difference was

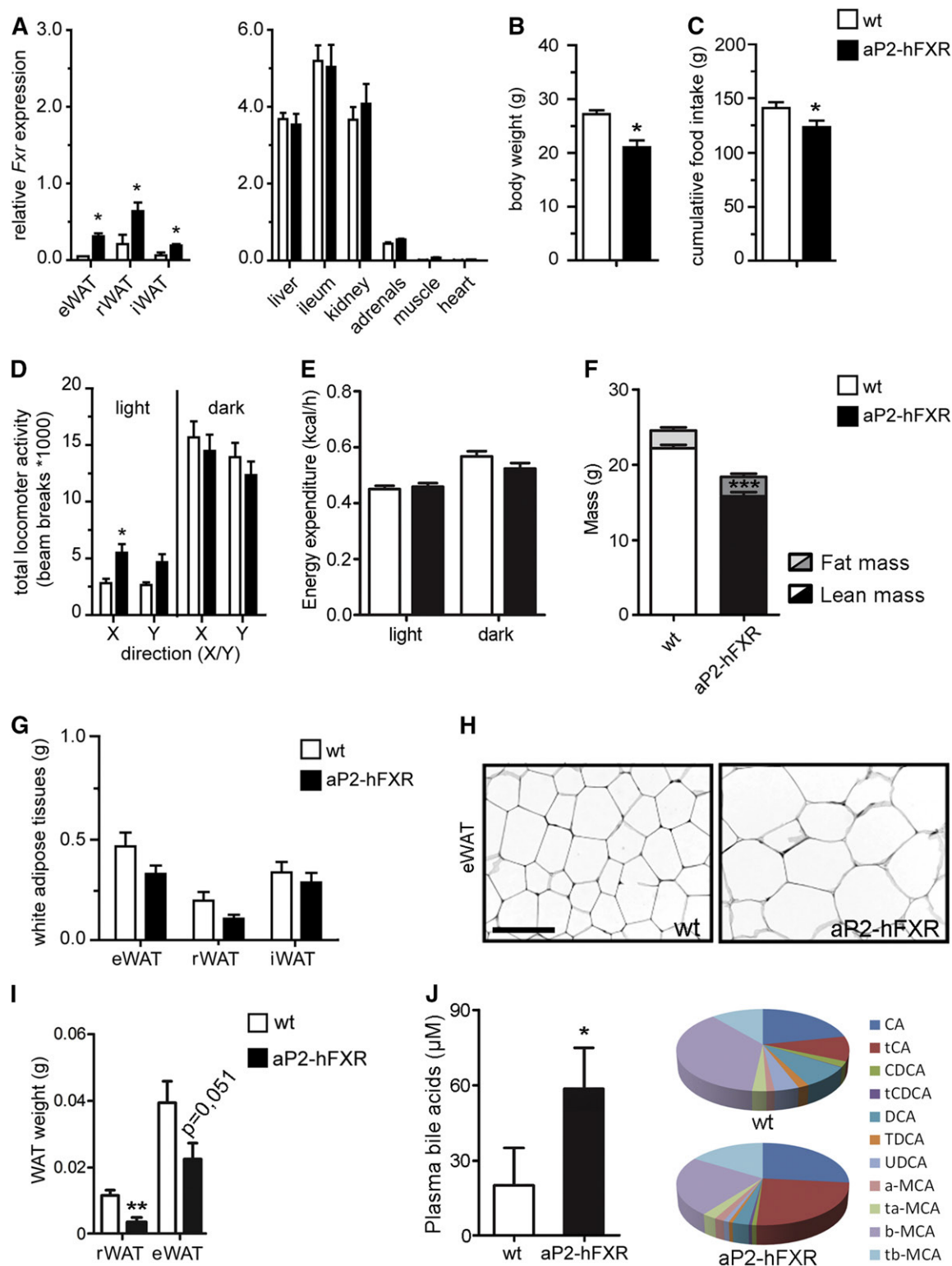


Fig. 1. Adipose *hFXR*-overexpressing mice are small and have hypertrophic adipocytes. **A:** Quantitative real-time PCR of total *FXR* expression in WAT depots (epididymal, retroperitoneal, and inguinal), liver, ileum, kidney, adrenals, muscle, and heart of wild-type (wt) and adipocyte-specific *FXR* overexpressing mice (aP2-hFXR). **B:** Body weight. **C:** Cumulative food intake from 6 to 13 weeks of age. **D:** Locomotor activity (D) of wild-type and aP2-hFXR mice. **E:** Energy expenditure at 21°C measured over 12 h light/12 h dark phase. **F:** Lean and fat mass after 13 weeks. **G:** WAT depot weights (G) and representative image of eWAT morphology showing adipocyte hypertrophy (H). **I:** Depot size of rWAT and eWAT 3 weeks after birth of wild-type and aP2-hFXR mice. **J:** Plasma bile acid composition and total amounts in wild-type and aP2-hFXR mice. Scale bar represents 100 μ m. All panels: $n = 6-8$ per group; data are represented as mean \pm SEM; * $P < 0.05$, ** $P < 0.01$, *** $P < 0.001$.

already apparent from weaning onwards (supplemental Fig. S1D). Surprisingly, the reduced weight of aP2-hFXR mice compared with controls was not only due to a reduction in fat mass; reduced lean body mass accounted for most of the difference (Fig. 1F). WAT depot weights of chow-fed aP2-hFXR mice were comparable to those in wild-type controls (Fig. 1G), particularly when normalized to body weight (data not shown). Histological examination of adipose tissues, however, revealed that adipocytes from chow-fed aP2-hFXR animals were markedly hypertrophic (Fig. 1H for eWAT, supplemental Fig. S1E for rWAT and iWAT).

To determine whether adipose tissue appearance is already affected early in development, WAT depots of very young aP2-hFXR mice were examined. Adipose depot development initiates just prior to birth and continues in the weeks thereafter, depending on the depot; and therefore, WAT of very young mice provides the opportunity to focus on adipose tissue that predominantly develops by adipogenesis (43). rWAT and eWAT weights of aP2-hFXR mice were decreased compared with wild-type controls already at 3 weeks of age (Fig. 1I), despite a comparable histological appearance (supplemental Fig. S1F). Taken together, these results indicate a role for FXR in early life WAT development and functioning.

As aP2-driven expression has been reported to also affect macrophages, depending on the size of the promotor in the construct and the integration site (44), we isolated intraperitoneal macrophages from aP2-hFXR and wild-type mice. Despite the fact that *hFXR* expression could indeed be detected, expression of inflammatory and FXR marker genes was not affected in these cells (supplemental Fig. S1G). Expression levels of monocyte chemoattractant protein 1 (*Mcp1*) and cluster of differentiation 68 (*Cd68*), a macrophage marker, were similar in eWAT of aP2-hFXR mice and controls (supplemental Fig. S1H), indicating no major effects of aP2-hFXR expression on macrophage attraction. To determine whether *hFXR* expression alters endocrine functions of adipose tissues, adipokine levels were analyzed in pooled plasma samples. We observed a 10–50% reduction in abundance for the majority of proteins that could be detected, including several adipokines that have been associated with inflammation and insulin resistance, such as dipeptidyl peptidase 4, soluble ICAM-1, macrophage colony-stimulating factor, pentraxin-2, and resistin (supplemental Fig. S1I). Also, the classical adipokines, leptin and adiponectin, showed decreased levels, whereas fibroblast growth factor 21 that positively affects several aspects of metabolic syndrome was one of the few proteins with increased abundance (+34%).

As bile acids are the natural ligands for FXR, we analyzed plasma bile acid levels and, unexpectedly, found elevated plasma bile acids in aP2-hFXR mice with altered composition. Particularly, substantially higher levels of cholate and taurocholate in the transgenic mice compared with controls were found (Fig. 1J). Hepatic expression levels of the major bile acid synthesis genes were analyzed, showing that *Cyp7a1* and *Cyp8b1* expression levels in aP2-hFXR mice were similar to those in control animals and, in line with this observation, no change in expression of small heterodimer

partner (*Shp*) (Nr0b2) was observed (supplemental Fig. S1J). Minor but significant decreases were observed for *Cyp27a1* (–18%) and *Cyp2c70* (–23%) mRNA levels. A more pronounced 2-fold decrease was observed in the expression levels of the hepatic bile acid uptake transporters *Ntcp* and *Oatp1a1* (supplemental Fig. S1J). Plasma aspartate transaminase (AST) levels were unaffected in aP2-hFXR mice, while alanine transaminase (ALT) showed a slight increase but remained very close to baseline (5 U/ml for controls and 14 U/ml for aP2-hFXR, data not shown).

Adipose FXR stimulates extracellular matrix remodeling

To further establish the physiological role of FXR in WAT, adipocyte size distribution was analyzed in the different depots. A clear shift in adipocyte size distribution as well as average adipocyte size was observed in chow-fed aP2-hFXR mice compared with controls (Fig. 2A, eWAT; supplemental Fig. S2A, rWAT and iWAT). As the reduced adipocyte size in *FXR*^{–/–} mice was one of the drivers of our initial interest toward investigating adipose FXR (24), aP2-hFXR mice were crossbred to whole-body *FXR* knockout mice. These mice showed similar aspects in their phenotype as *hFXR* adipose overexpressors on the wild-type background did, including ~20–30% lower body weights, stemming from reduced lean mass (supplemental Fig. S2B) and comparable locomotor activity and energy expenditure as *FXR*^{–/–} controls (supplemental Fig. S2C, D). Adipose depot weights of *FXR*^{–/–} aP2-hFXR mice were similar to those of controls (Fig. 2B); yet, adipocyte hypertrophy was again apparent (Fig. 2C, supplemental Fig. S2E). This hypertrophy was, however, somewhat less pronounced when compared with the hFXR-induced phenotype in the wild-type background (Fig. 2D, supplemental Fig. S2E, F).

To gain insight in the mode(s) of action by which the transcription factor FXR acts in WAT, Affymetrix microarray analysis was performed on eWAT samples obtained from chow-fed aP2-hFXR and wild-type mice. A total of 1,372 genes were found to be differentially expressed. Annotation analysis using DAVID and GSEA showed that among the most significantly affected cellular components and enriched gene sets, the extracellular matrix (ECM) seemed to be clearly affected by the presence of aP2-hFXR (Fig. 3A). Several collagen-encoding genes were upregulated, including the collagen VI (but not the endotrophin-encoding $\alpha 3$ type), collagen I, IV, and XV genes, as well as other ECM factors like elastin, biglycan, and lumican, and ECM-modifying genes, such as cathepsins and metalloproteinases (supplemental Table S1).

Altered expression or activity of the master regulators of adipogenesis, *PPAR γ* and CAAT/enhancer-binding protein (*C/EBP α*), could in theory account for the inability of adipose depot expansion in aP2-hFXR mice. A 26% and 33% reduction in expression of these genes was observed. However, no striking differential expression of *PPAR γ* target genes between the groups was observed (supplemental Table S2). Wnt/ β -catenin signaling has been shown to be increased in *FXR*^{–/–} mice. In line with the reported downregulation of secreted inhibitors of Wnt signaling, *Sfrp1* and *Sfrp5*, in *FXR*^{–/–} mice (26), we observed upregulation

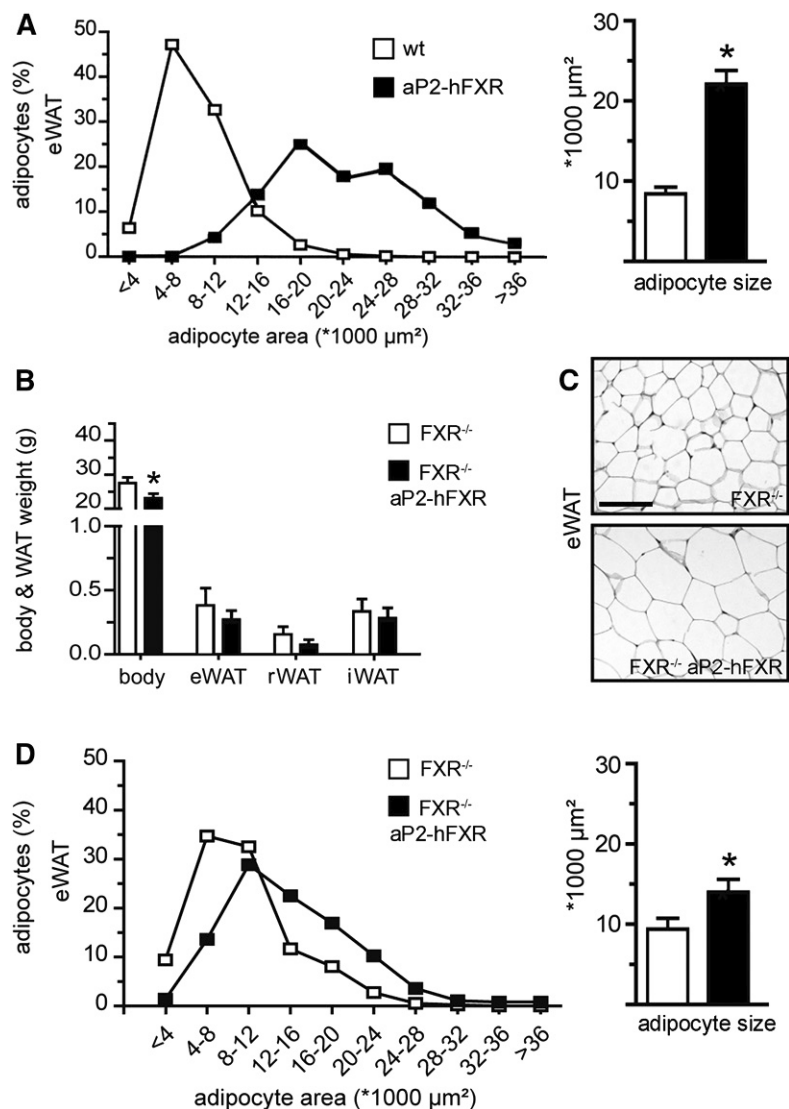


Fig. 2. Adipose *hFXR* increases adipocyte size without affecting adipose depot size. **A:** Distribution of adipocyte size (in percentage) in eWAT and average adipocyte size in wild-type (wt) and aP2-hFXR mice. **B:** Body and WAT weight (**B**), eWAT morphology (**C**), and distribution and average adipocyte size (**D**) of FXR^{-/-} and FXR^{-/-} aP2-hFXR mice. All panels: n = 6–8 per group; data are represented as mean \pm SEM; **P* < 0.05. Scale bar represents 100 μm .

(2.01-fold and 2.65-fold, respectively) of these genes in eWAT of aP2-hFXR mice. However, downregulation of Wnt signaling target genes, as observed in vitro in pre-adipocytes (26), was not evident (supplemental Table S2). In line with the unaltered expression levels of *Mcp1* and *Cd68* (see supplemental Fig. S1H), eWAT transcriptomics showed no differential expression of established inflammation markers.

To assess the role of FXR in ECM remodeling in more detail, quantitative profiling of the eWAT secretome was performed ex vivo. This approach resulted in identification of several proteins that were either more abundant or exclusively present in WAT from aP2-hFXR mice. Only a limited number of proteins showed a decreased abundance (Fig. 3B, supplemental Tables S3, S4) (40).

Overrepresentation of specific collagen families, such as fibril-forming collagens (COL1A1, COL5A2), fibril-associated collagens (FACIT; COL14A1, COL15A1), and beaded filament-forming collagens (COL6A1, COL6A5), and ECM components like laminin, fibronectin, biglycans, dermatopontin, and cadherin-5 were observed in aP2-hFXR WAT secretomes, in line with the outcome of the transcriptome analysis.

To determine whether the observed increase in ECM protein synthesis actually leads to fibrosis in vivo and is not compensated by ECM degradation, specific fibrosis staining was performed on eWAT and iWAT harvested from both chow-fed wild-type and FXR^{-/-} mice expressing aP2-hFXR and compared with the respective controls. Disorganized ECM was apparent in iWAT from the transgenic mice with loss of the characteristic septa that subdivide the tissue into subsections (Fig. 4A, supplemental Fig. S3) (45). In eWAT, accumulation of collagen was observed that predominantly surrounded individual adipocytes (i.e., pericellular fibrosis, Fig. 4B, supplemental Fig. S3). The COL1A1 protein level was also elevated in the eWAT of FXR^{-/-} aP2-hFXR mice and, in line with the secretome analysis (see Fig. 3), COL1A2 was not (Fig. 4C, D). Lamin-A, a protein that scales with tissue stiffness (46), was increased as well (Fig. 4C, D).

FXR expression in adipose tissue leads to redistribution of body fat during HFD feeding

Next, we examined the effects of *hFXR* overexpression on WAT functioning in mice with a positive energy balance

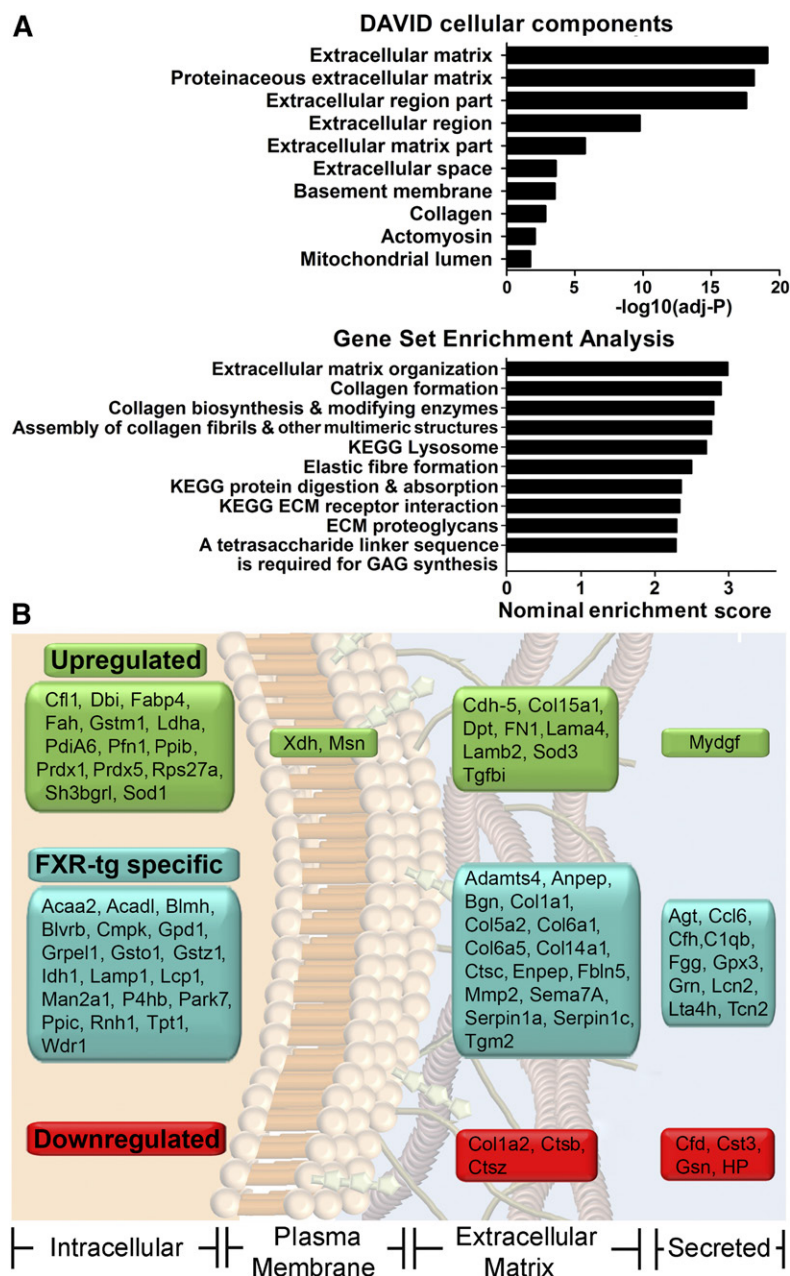


Fig. 3. Adipose *hFXR* affects transcriptional and translational processes associated with the ECM formation. **A:** Functional annotation categorization of aP2-hFXR versus wild-type eWAT transcriptomics, showing David top 10 of enriched cellular components and GSEA. **B:** Secretome analysis of eWAT ex vivo showing statistically significant decreased/increased protein levels as well as aP2-hFXR-specific proteins identified according to cellular localization.

induced by feeding a HFD for 6 weeks (60% of calories from fat). Whereas WAT depots of control mice expanded (~ 2.5 -fold, **Fig. 5A**), those of aP2-hFXR mice remained similar in size to chow-fed conditions (only 1.1- to 1.4-fold expansion, compare dotted line to bar). Adipocytes from HFD-fed wild-type mice were markedly larger than those from mice fed on chow, while adipocytes from aP2-hFXR mice remained as hypertrophic as observed during chow-fed conditions (**Fig. 5B, C**; supplemental **Fig. S4A**). Both absorption of dietary fat and locomotor activity were unaffected and, in contrast to chow-fed conditions, cumulative food intake was similar in both groups (supplemental **Fig. S4B–D**). No differences in energy expenditure were observed between the groups either (supplemental **Fig. S4E**). This unexpected inability for WAT to expand was subsequently also observed in an ageing experiment. The mass

of WAT compartments was significantly increased by ~ 2.5 -fold in aged (1 year old) chow-fed wild-type mice when compared with 14-week-old mice. In contrast, ageing of aP2-hFXR mice hardly induced any expansion of WAT depots that, like the aged controls, contained hypertrophic adipocytes with even smaller size compared with young aP2-hFXR mice (**Fig. 5D–F**, supplemental **Fig. S4F**).

FXR $^{-/-}$ mice were shown to be resistant to diet-induced obesity (27), and FXR $^{-/-}$ aP2-hFXR mice were therefore also fed the HFD. This resulted in similar weight gains (5.0 g or 19% vs. 5.3 g or 23% for FXR $^{-/-}$ and FXR $^{-/-}$ aP2-hFXR mice, respectively; **Fig. 5G**), indicating that adipocytic *Fxr* is not responsible for the suppressive effect of *Fxr* ablation on development of diet-induced obesity. aP2-driven FXR overexpression in the FXR $^{-/-}$ background did result in a small but significant increase in adipocyte size in eWAT

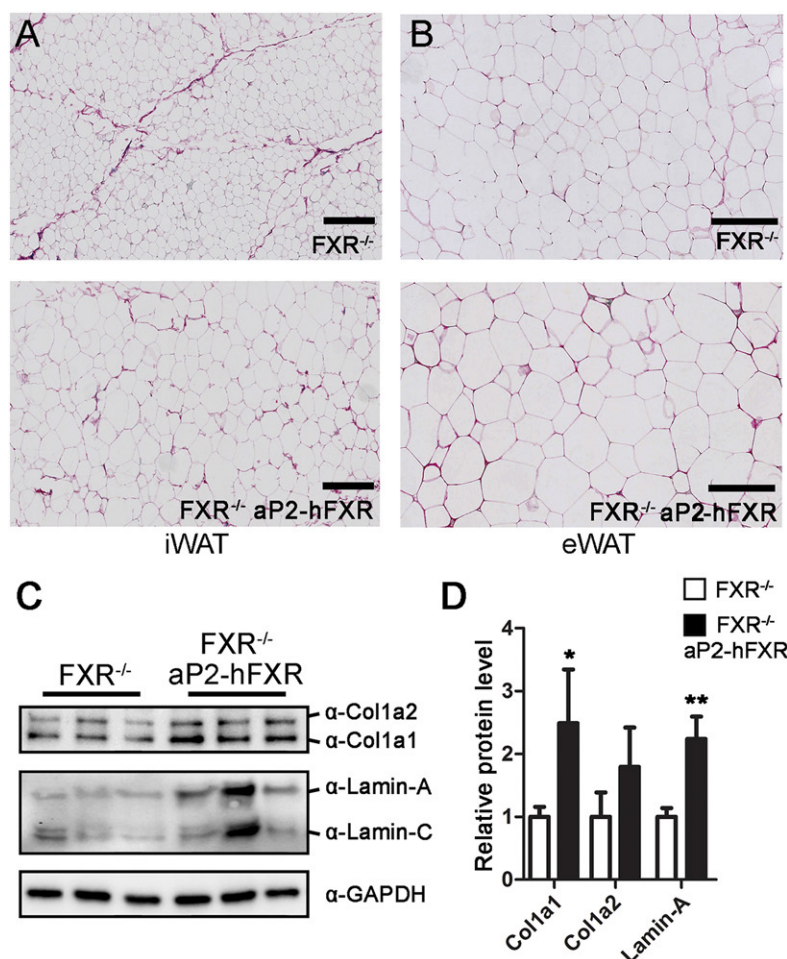


Fig. 4. Adipose *hFXR* causes collagen deposition and alters adipose architecture. Collagen characterization in iWAT (A) and eWAT (B) of chow-fed FXR^{-/-} and FXR^{-/-} aP2-hFXR mice by picrosirius red staining. Collagen I and lamin-A/C protein levels (C) and quantification in eWAT of chow-fed FXR^{-/-} and FXR^{-/-} aP2-hFXR mice (D) (n = 6; data are represented as mean ± SEM; *P < 0.05, **P < 0.01). Scale bar represents 200 μm.

and iWAT but not in rWAT after 6 weeks of HFD (Fig. 5H, I; supplemental Fig. S4G). Adipose depot size, however, remained similar to chow-fed conditions and lacked the expansion observed in FXR^{-/-} controls (Fig. 5G). Fibrosis staining again showed a disorganized ECM in iWAT of FXR^{-/-} aP2-hFXR mice; however, as expected, septa were also not readily observed in FXR^{-/-} controls after HFD (Fig. 5J). Similar to chow-fed mice, fibrosis staining was more pronounced in eWAT of FXR^{-/-} aP2-hFXR mice, however, in FXR^{-/-} control animals also, fibrotic patches became apparent after HFD feeding, as occurs in wild-type animals as well (Fig. 5K) (45). In line with the above, the increased expression of ECM-encoding genes observed in eWAT of chow-fed aP2-hFXR mice was not apparent anymore after HFD in eWAT of FXR^{-/-} aP2-hFXR compared with FXR^{-/-} controls with only a trend for increased *Col1a1*. This implies that the development of fibrosis occurred already early during development on standard chow conditions and is matched by the control animals during a positive energy balance (supplemental Fig. S4H). Similar to the unaltered expression of inflammatory markers in eWAT and macrophages on the wild-type background, expression of *Cd68*, *Tnfa*, *Mcp1*, and *Il10* in eWAT and liver of chow- or HFD-fed FXR^{-/-} aP2-hFXR mice was not altered compared with controls. Crown-like structure abundance also remained unaffected (supplemental Table S5).

Adipocytic FXR-induced ectopic lipid accumulation aggravates insulin resistance

To determine whether the impaired expansion capacity of adipose depots in aP2-hFXR mice has adverse metabolic consequences, lipid contents in plasma and organs were analyzed. Plasma free fatty acids tended to be elevated in chow-fed FXR^{-/-} aP2-hFXR mice when compared with FXR^{-/-} controls and were significantly elevated after HFD (Fig. 6A). Free fatty acids were also elevated in aP2-hFXR mice on wild-type background relative to controls both on chow and on HFD (supplemental Fig. S5A). After HFD feeding for 6 weeks, ectopic lipid accumulation in both liver and muscle tended to occur in hFXR-overexpressing mice on wild-type background as well, indicating that limitation of adipose depot expansion capacity due to the presence of adipocytic hFXR leads to ectopic fat accumulation, particularly in the liver (supplemental Fig. S5B–D). Of note, the livers of chow-fed aP2-hFXR mice appeared to be very similar to those of control animals, as confirmed by the absence of elevated aminotransferases in plasma and histological signs of liver damage. To exclude potential contributions of unknown indirect effects on hepatic lipid accumulation, e.g., due to dysregulation of hepatic acetyl-CoA metabolism leading to excess hepatic lipogenesis (47), the origin of hepatic fatty acids was determined. Quantification of de novo lipogenesis in vivo by a mass isotope distribution analysis approach (48) revealed the

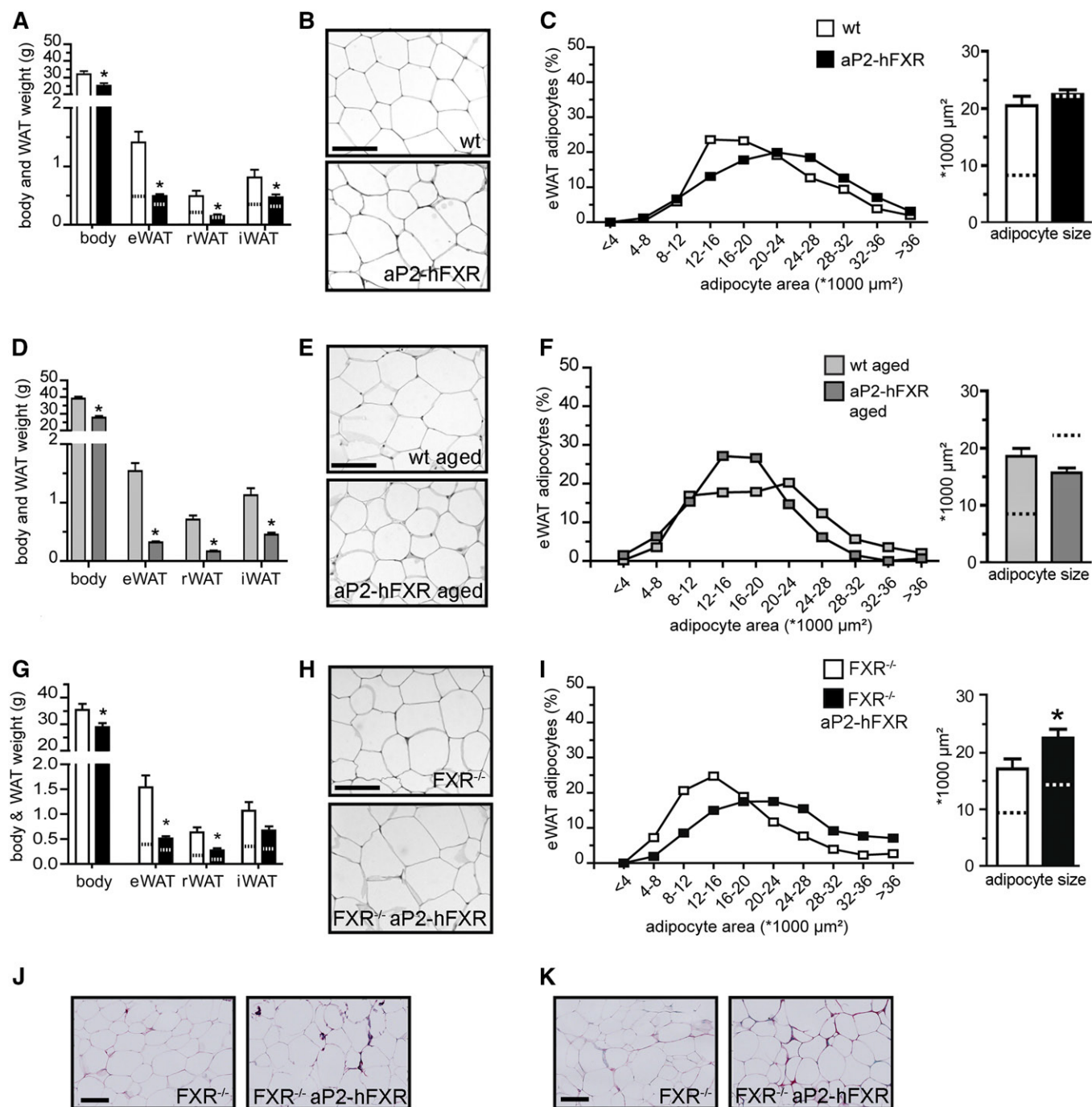


Fig. 5. HFD prevents further growth of hypertrophic adipocytes in aP2-hFXR mice and fat depot expansion is limited. **A:** Body and WAT weight of wild-type (wt) and aP2-hFXR mice after 6 weeks of HFD. The dotted lines indicate WAT weights of chow-fed mice (presented in Fig. 1). **eWAT morphology (B)** and distribution and average of adipocyte size (C) after 6 weeks of HFD. **D:** Body and WAT weight of 1-year-old chow-fed wild-type and aP2-hFXR mice. **eWAT morphology (E)** and distribution and average adipocyte size (F) of 1-year-old wild-type and aP2-hFXR mice. **G:** Body and WAT weight of $\text{FXR}^{-/-}$ aP2-hFXR mice after 6 weeks of HFD. Dotted lines indicate weights of chow-fed control animals (depicted in Fig. 2). **eWAT morphology (H)** and distribution of adipocyte size and average adipocyte size (I) of $\text{FXR}^{-/-}$ aP2-hFXR mice after 6 weeks of HFD. Sirius red fibrosis staining of iWAT (J) and eWAT (K) after 13 weeks of HFD ($n = 6-9$ per group; data are represented as mean \pm SEM; $*P < 0.05$). Scale bar represents 100 μm .

presence of virtually identical amounts of fatty acids derived from de novo lipogenesis and from chain elongation, indicating that stimulation of these pathways does not drive the accumulation of hepatic triglycerides in aP2-hFXR mice on HFD (supplemental Fig. S5E). This observation, combined with elevated free fatty acid levels in plasma,

strongly suggests that hepatic fat accumulation is due to an overflow from adipocytic fat stores.

A similar trend in hepatic triglyceride accumulation after 6 weeks on HFD was observed in $\text{FXR}^{-/-}$ aP2-hFXR mice compared with $\text{FXR}^{-/-}$ controls (supplemental Fig. S5F, G). To elaborate on these metabolic consequences, we next

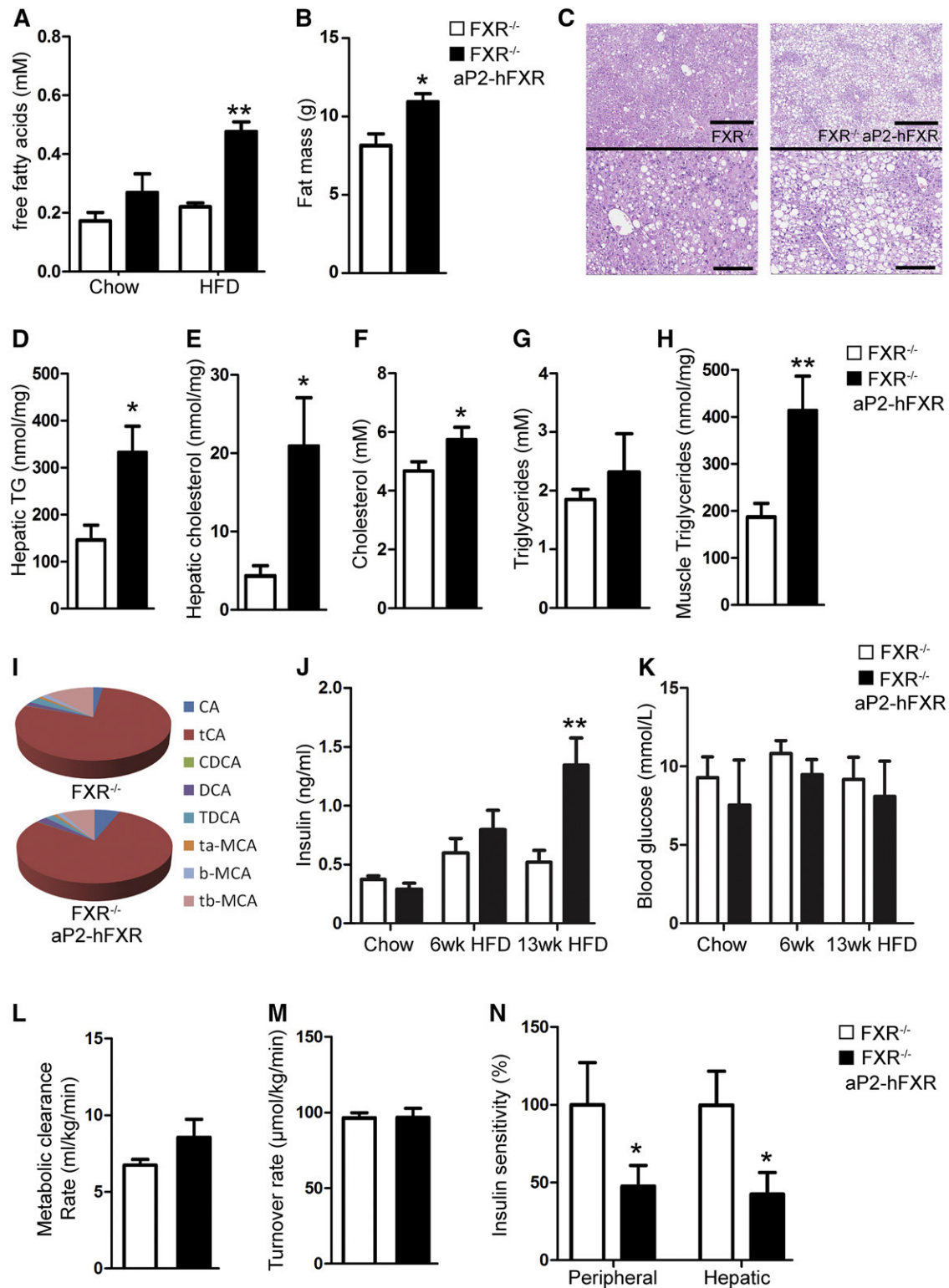


Fig. 6. Obesogenic conditions induce ectopic lipid accumulation and insulin resistance in aP2-hFXR mice. A: Plasma free fatty acid levels of chow- and HFD-fed FXR^{-/-} and FXR^{-/-} aP2-hFXR mice. B: Fat mass of FXR^{-/-} and FXR^{-/-} aP2-hFXR mice after 3 months of HFD. C: Liver H&E staining showing lipid accumulation that is most apparent in the pericentral zone. Top scale bars in panel C depict 500 μm, bottom scale bars in enlargements depict 200 μm. Hepatic triglycerides (D) and hepatic total cholesterol (E) of FXR^{-/-} and FXR^{-/-} aP2-hFXR mice after prolonged HFD. Plasma total cholesterol (F) and triglycerides (G) of FXR^{-/-} and FXR^{-/-} aP2-hFXR mice after 3 months of HFD. Gastrocnemius triglycerides of FXR^{-/-} and FXR^{-/-} aP2-hFXR mice after 3 months of HFD (H) and plasma bile acid composition (I). (J) Four hour-fasted plasma insulin (J) and blood glucose (K) of chow- and HFD-fed FXR^{-/-} and FXR^{-/-} aP2-hFXR mice. Metabolic clearance rate (L), turnover rate (that under these conditions equals glucose production) (M), and peripheral and hepatic insulin sensitivity (N) during a whole-body glucose test of FXR^{-/-} and FXR^{-/-} aP2-hFXR mice after 3 months of HFD (n = 6–8 per group; data are represented as mean ± SEM; *P < 0.05, **P < 0.01, ***P < 0.001).

extended the duration of a positive energy balance to 3 months in $\text{FXR}^{-/-}$ and $\text{FXR}^{-/-}$ aP2-hFXR mice, because $\text{FXR}^{-/-}$ mice have been reported to be resistant to diet-induced obesity (27). To test whether these mice simply store less fat, total fat mass was determined by MRI, which showed that more fat actually accumulated in $\text{FXR}^{-/-}$ aP2-hFXR mice than in $\text{FXR}^{-/-}$ controls after this prolonged period of HFD feeding (Fig. 6B). Within this period, significantly more triglycerides and cholesterol accumulated in the livers of $\text{FXR}^{-/-}$ aP2-hFXR mice than in those of $\text{FXR}^{-/-}$ mice (Fig. 6C–E).

Plasma cholesterol levels were slightly elevated in $\text{FXR}^{-/-}$ aP2-hFXR mice, whereas plasma triglycerides remained similar to those in $\text{FXR}^{-/-}$ controls (Fig. 6F, G). Muscle triglyceride content was significantly elevated in $\text{FXR}^{-/-}$ aP2-hFXR mice after 3 months on HFD (Fig. 6H). The $\text{FXR}^{-/-}$ aP2-hFXR mice tended toward elevated plasma bile acids after 3 months on HFD, but were not altered, most probably due to the known dominant effect of whole-body FXR ablation that shifts the bile acid composition toward predominantly taurocholate in both groups (Fig. 6I, supplemental Fig. S5I) (49, 50). The differences in adipose depot size between both groups remained similar to the differences observed after 6 weeks of HFD feeding, indicating that the storage capacity of WAT depots rapidly became limiting in the $\text{FXR}^{-/-}$ aP2-hFXR mice; whereas in the $\text{FXR}^{-/-}$ control animals, the positive energy balance could largely be matched by adipose storage capacity during the experiment (supplemental Fig. S5J).

Ectopic lipid accumulation, accompanied by increased concentrations of intermediates of lipid metabolism, such as diacylglycerols and ceramides, is one of the drivers of insulin resistance (51). Therefore, we analyzed glucose kinetics by a dynamic stable isotope test. Compared with $\text{FXR}^{-/-}$ controls, HFD-fed $\text{FXR}^{-/-}$ aP2-hFXR mice showed similar blood glucose levels; yet, insulin levels were 3-fold higher (Fig. 6J, K). Of note, after 6 weeks of HFD, insulin levels were unaltered in $\text{FXR}^{-/-}$ aP2-hFXR mice compared with controls (also on the wild-type background, supplemental Fig. S5K, L) indicating that the lack of adipose expansion capacity precedes elevated insulin levels after prolonged obesogenic conditions. Determination of glucose kinetics under normoglycemic conditions, using a stable isotopically labeled glucose tracer (34), showed that metabolic clearance rates and glucose production rates were similar in $\text{FXR}^{-/-}$ aP2-hFXR and $\text{FXR}^{-/-}$ control mice, yet, at the expense of 3-fold increased insulin levels due to a marked hepatic and peripheral insulin resistance (Fig. 6L–N). Overall, these data indicate that moderate aP2-controlled overexpression of human FXR in fat tissues results in adipocyte hypertrophy and limited WAT expansion capacity when challenged with HFD, leading to ectopic lipid accumulation and insulin resistance.

DISCUSSION

The studies presented here establish that the bile acid-activated nuclear receptor, FXR, may contribute to the regulation of fat tissue function and architecture. We show

that transgenic mice that moderately overexpress *hFXR* (3- to 5-fold compared with endogenous *Fxr*) under the control of the aP2 (*Fabp4*) promoter have WAT with enlarged adipocytes under standard chow-fed conditions. On a HFD as well as at a moderately old age, these mice show very limited expansion of WAT depots and an inability to further increase adipocyte size. In accordance with a limited storage capacity of WAT due to this localized *FXR* overexpression, ectopic lipid deposition occurred during conditions of a positive energy balance on both wild-type and whole-body $\text{FXR}^{-/-}$ backgrounds. Extensive ECM remodeling was observed and may be involved in this unexpected action of FXR in regulating adipose tissue architecture. It is of importance to note that the expression levels of *hFXR* in adipose tissues reached in our models were still low compared with the expression of endogenous *Fxr* in liver and intestine, at least at the RNA level. This may reflect a low expression per adipocyte or, alternatively, expression in a subset of cells. It is evident that additional studies, e.g., by employing adipose-specific FXR-deficient mouse models, are warranted to unequivocally establish the (patho)physiological role of FXR in adipose biology.

Although the temporal dynamics of expansion differ for specific WAT depots and different developmental stages have distinct molecular underpinnings of adipogenesis (43, 52, 53), *hFXR*-associated hypertrophy and limited expansion capacity were observed in all depots analyzed and at different ages of the mice, suggesting a fundamental role for this nuclear receptor in adipose biology. In line with the “critical fat cell size” hypothesis (54), the hypertrophic adipocytes in aP2-hFXR mice did not increase further in size during a positive energy balance, and depot size also did not increase; therefore, hyperplasia must be suppressed under these conditions. This was confirmed by the reduced depot size of FXR-overexpressing mice shortly after birth; although FXR has been proposed to be a positive regulator of adipogenesis *in vitro* (25, 26). The adipose micro-environment in the *in vivo* situation therefore seems to predominate over potential positive effects of FXR activity on adipogenesis; however, to confirm that FXR does not affect Wnt signaling *in vivo* requires a more thorough investigation of pre-adipocytes in WAT.

Interestingly, prolonged treatment with an FXR agonist during obesogenic conditions also seems to result in adipocyte hypertrophy (55). The observation that, in aged mice overexpressing *hFXR*, expansion of adipose depots was also limited and that adipocyte size in eWAT was even decreased compared with young mice (compare Fig. 2A to Fig. 5F) is in line with inhibition of adipose plasticity upon *FXR* overexpression. The eWAT depot is known to have a high dependency on newly formed cells, a process that declines with age (56, 57). *Fxr* expression was reported to decrease in WAT during genetic and diet-induced obesity in mice (24). We now provide suggestive evidence that this effect may in fact liberate WAT plasticity, providing increased storage capacity upon excessive energy intake.

The wild-type and $\text{FXR}^{-/-}$ backgrounds did result in subtle differences concerning the effects on WAT expansion and adipocyte size by FXR overexpression (i.e., compare

Fig. 5C to Fig. 5I), suggesting that external FXR-mediated cues on adipose FXR function do exist. Of note, although the reported reduced adipocyte size in $\text{FXR}^{-/-}$ mice was one of the major reasons for us to focus on adipocytic FXR (24), the complete FXR knockout model used in this study displayed similar adipocyte size as wild-type mice did (compare Fig. 2A to Fig. 2D) (50), and thus lacked the smaller adipocytes observed earlier in $\text{FXR}^{-/-}$ mice generated by Cre-mediated deletion of the last exon (24). Possibly, the latter model might still produce a truncated form of FXR that contains the DNA-binding domain (50). When comparing the wild-type and FXR-deficient backgrounds, however, the large shift in bile acid pool size and composition due to lack of hepatic and intestinal FXR could affect the function of adipose FXR, as ligand availability in plasma is dramatically altered (58). As observed previously (59), we also identified expression of organic anion transporting polypeptide 2B1 (*Oatp2b1*; *Slc2b1*), a transporter with ubiquitous expression that may facilitate adipocytic bile acid uptake. Unexpectedly, adipose *FXR* overexpression resulted in elevated plasma bile acids with a more hydrophobic composition, which may generate a feedforward loop toward adipose FXR activation. Analysis of expression of hepatic bile acid synthesis genes on which both intestinal and hepatic FXR activity converges, revealed only a minor reduction in *Cyp7b1*, *Cyp27a1*, and *Cyp2c70* and no effect on *Shp* expression or the major bile acid synthesis genes, *Cyp7a1* and *Cyp8b1*, that are regulated by SHP downstream of hepatic FXR.

Yet, *Ntcp* and *Oatp1a1* were over 2-fold downregulated, suggesting that impaired hepatic uptake of bile acids is responsible for the observed accumulation of bile acids in plasma. The underlying mechanism hereof, suggesting adipose-liver cross-talk, remains elusive. Adipose tissue formation during late fetal and early postnatal life in humans is highly sensitive to the nutritional environment and coincides with the period of so-called “physiological cholestasis” in newborns (elevated plasma concentrations of primary bile acids) (60). Bile acids acting as an endogenous ligand for FXR in adipose tissue that contribute to regulation of adipogenesis are therefore of potential importance during this stage of development.


Adipose transcriptomics and ex vivo secretome analysis revealed broad changes in the adipose ECM upon *FXR* overexpression. Recent interest in the cues that determine the fate of stem cells toward a specific lineage have underlined the importance of the microenvironment in which these cells reside and, in particular, the properties of the ECM (61). The stiffness of the matrix defines the plasticity of the stem cell/pre-adipocyte population: nuclear lamin A, a component of one of the mechano-sensing mechanisms, strongly scales with tissue stiffness (46). Mastering these parameters of the microenvironment in which stem cells are directed toward a desired fate has been instrumental in enabling stem cell research, tissue regeneration, and the production of organoids (62). Also in adipose tissue, ECM homeostasis and remodeling according to prevailing tissue needs is an important high-maintenance process, which is particularly evident in mature adipocytes (63).

Based on our results, we propose that FXR-induced alterations in ECM homeostasis (co-)dictate adipocyte hyperplasia and fat depot expansion. Control of the adipocyte microenvironment has recently also been shown to be regulated by a specific subset of adipocyte progenitors (64). These cells, which are positive for platelet-derived growth factor receptor α or β , seem to derive from a common progenitor as pre-adipocytes destined to mature into adipocytes. These cells therefore seem to be at the crossroad between healthy and unhealthy adipose tissue development (65, 66). Despite the fact that the adiponectin promotor has become the preferred tool for generating adipocyte-specific knockout mice, the aP2-driven model applied in this study has the advantage that it also targets the adipocyte precursors. Whether FXR already alters the developmental trajectory of these progenitors with increased tissue stiffness as a consequence or acts further down the line, for instance by altering this lamin A-based sensing mechanism (67), remains to be established.

Paradoxically, the Scherer laboratory revealed that, next to its infamous role in metabolic disease, inflammation of adipose tissue is actually required for healthy expansion as well (68). Although the level of expression in adipose tissue is more than 1,000-fold higher than in adipose-resident macrophages (69), we were able to detect *hFXR* mRNA in isolated macrophages in our model. However, no effect was observed on inflammatory markers or the abundance of crown-like structures, or even on the expression of FXR target genes in macrophages, strongly suggesting that the off-target expression is very limited; although we cannot definitely rule out a role for macrophage FXR. One phenomenon in our model that could possibly be explained by non-adipocyte expression is the highly intriguing reduction in lean body mass. Although we think that it is tempting to speculate that an adipocyte-derived factor is causal to this phenotype, we were unable to identify major changes in known adipokines that regulate lean mass development. Further studies are therefore required to determine the cause of this highly interesting phenotype.

The increased plasma free fatty acid levels that were observed already under chow-fed conditions suggests that WAT storage capacity is limited but can systemically still be compensated for. Yet, exposure to a positive energy balance provokes ectopic lipid accumulation in liver and muscle. As adipose-derived fatty acid flux contributes 60–80% of the hepatic lipid influx in both mice and men, subtle changes in adipose output may lead to severe hepatic consequences over time (70, 71). Recently, for instance, adipose tissue lipolysis rates were found to drive hepatic glucose production (47). The observed elevated plasma levels of free fatty acids in our model, indicative of an increased rate of lipolysis, did not lead to increased glucose production. Yet, ectopic lipid accumulation was associated with evident insulin resistance, which delineates a pathophysiological relevance for adipocytic FXR in whole-body energy metabolism.

In conclusion, our studies establish that the nuclear receptor, FXR, is a determinant of fat tissue function and architecture, among others, by control of ECM remodeling, which adds to the extended list of FXR functionalities

(2, 5). Our work thus provides new insights into the contribution of FXR in the maintenance of whole-body energy balance, in addition to its better understood functions in liver and intestine. In view of the current development of FXR agonists for treatment of human metabolic diseases, potential fat-specific actions of these compounds must be considered. 

Mouse α P2 promoter and human FXR α 2-expressing plasmids were kindly provided by Dr. R. E. Hammer (Department of Biochemistry and the Howard Hughes Medical Institute, University of Texas Southwestern Medical Center, Dallas, TX) and Dr. R. Mukherjee (Bristol-Myers Squibb Company, Experimental Station, Wilmington, DE).

REFERENCES

- Lefebvre, P., B. Cariou, F. Lien, F. Kuipers, and B. Staels. 2009. Role of bile acids and bile acid receptors in metabolic regulation. *Physiol. Rev.* **89**: 147–191.
- Hegyi, P., J. Mal  th, J. R. Walters, A. F. Hofmann, and S. J. Keely. 2018. Guts and gall: bile acids in regulation of intestinal epithelial function in health and disease. *Physiol. Rev.* **98**: 1983–2023.
- Kuipers, F., V. W. Bloks, and A. K. Groen. 2014. Beyond intestinal soap–bile acids in metabolic control. *Nat. Rev. Endocrinol.* **10**: 488–498.
- Shapiro, H., A. A. Kolodziejczyk, D. Halstuch, and E. Elinav. 2018. Bile acids in glucose metabolism in health and disease. *J. Exp. Med.* **215**: 383–396.
- Massafra, V., and S. W. van Mil. 2018. Farnesoid X receptor: A “homeostat” for hepatic nutrient metabolism. *Biochim. Biophys. Acta Mol. Basis Dis.* **1864**: 45–59.
- Nevens, F., P. Andreone, G. Mazzella, S. I. Strasser, C. Bowlus, P. Invernizzi, J. P. Drenth, P. J. Pockros, J. Regula, U. Beuers, et al.; POISE Study Group. 2016. A placebo-controlled trial of obeticholic acid in primary biliary cholangitis. *N. Engl. J. Med.* **375**: 631–643.
- Mudaliar, S., R. R. Henry, A. J. Sanyal, L. Morrow, H. U. Marschall, M. Kipnes, L. Adorini, C. I. Sciacca, P. Clopton, E. Castellote, et al. 2013. Efficacy and safety of the farnesoid X receptor agonist obeticholic acid in patients with type 2 diabetes and nonalcoholic fatty liver disease. *Gastroenterology*. **145**: 574–582.e1.
- Neuschwander-Tetri, B. A., R. Loomba, A. J. Sanyal, J. E. Lavine, M. L. van Natta, M. F. Abdelmalek, N. Chalasani, S. Dasarthy, A. M. Diehl, B. Hameed, et al.; NASH Clinical Research Network. 2015. Farnesoid X nuclear receptor ligand obeticholic acid for non-cirrhotic, non-alcoholic steatohepatitis (FLINT): a multicentre, randomised, placebo-controlled trial. *Lancet*. **385**: 956–965.
- Tully, D. C., P. V. Rucker, D. Chianelli, J. Williams, A. Vidal, P. B. Alper, D. Mutnick, B. Bursulaya, J. Schmeits, X. Wu, et al. 2017. Discovery of tropifexor (LJN452), a highly potent non-bile acid FXR agonist for the treatment of cholestatic liver diseases and nonalcoholic steatohepatitis (NASH). *J. Med. Chem.* **60**: 9960–9973.
- Ch  vez-Talavera, O., A. Tailleux, P. Lefebvre, and B. Staels. 2017. Bile acid control of metabolism and inflammation in obesity, type 2 diabetes, dyslipidemia, and nonalcoholic fatty liver disease. *Gastroenterology*. **152**: 1679–1694.e3.
- Han, C. Y. 2018. Update on FXR biology: promising therapeutic target? *Int. J. Mol. Sci.* **19**: E2069.
- Kowdley, K. V., V. Luketic, R. Chapman, G. M. Hirschfield, R. Poupon, C. Schramm, C. Vincent, C. Rust, A. Par  s, A. Mason, et al.; Obeticholic Acid PBC Monotherapy Study Group. 2018. A randomized trial of obeticholic acid monotherapy in patients with primary biliary cholangitis. *Hepatology*. **67**: 1890–1902.
- Makishima, M., A. Y. Okamoto, J. J. Repa, H. Tu, R. M. Learned, A. Luk, M. V. Hull, K. D. Lustig, D. J. Mangelsdorf, and B. Shan. 1999. Identification of a nuclear receptor for bile acids. *Science*. **284**: 1362–1365.
- Parks, D. J., S. G. Blanchard, R. K. Bledsoe, G. Chandra, T. G. Consler, S. A. Kliewer, J. B. Stimmel, T. M. Willson, A. M. Zavacki, D. D. Moore, et al. 1999. Bile acids: natural ligands for an orphan nuclear receptor. *Science*. **284**: 1365–1368.
- Wang, H., J. Chen, K. Hollister, L. C. Sowers, and B. M. Forman. 1999. Endogenous bile acids are ligands for the nuclear receptor FXR/BAR. *Mol. Cell.* **3**: 543–553.
- Goodwin, B., S. A. Jones, R. R. Price, M. A. Watson, D. D. McKee, L. B. Moore, C. Galardi, J. G. Wilson, M. C. Lewis, M. E. Roth, et al. 2000. A regulatory cascade of the nuclear receptors FXR, SHP-1, and LRH-1 represses bile acid biosynthesis. *Mol. Cell.* **6**: 517–526.
- Inagaki, T., M. Choi, A. Moschetta, L. Peng, C. L. Cummins, J. G. McDonald, G. Luo, S. A. Jones, B. Goodwin, J. A. Richardson, et al. 2005. Fibroblast growth factor 15 functions as an enterohepatic signal to regulate bile acid homeostasis. *Cell Metab.* **2**: 217–225.
- Cariello, M., E. Piccinin, O. Garcia-Irigoyen, C. Sabb  , and A. Moschetta. 2018. Nuclear receptor FXR, bile acids and liver damage: Introducing the progressive familial intrahepatic cholestasis with FXR mutations. *Biochim. Biophys. Acta Mol. Basis Dis.* **1864**: 1308–1318.
- Zhang, Y., H. R. Kast-Woelbern, and P. A. Edwards. 2003. Natural structural variants of the nuclear receptor farnesoid X receptor affect transcriptional activation. *J. Biol. Chem.* **278**: 104–110.
- Kusminski, C. M., P. E. Bickel, and P. E. Scherer. 2016. Targeting adipose tissue in the treatment of obesity-associated diabetes. *Nat. Rev. Drug Discov.* **15**: 639–660.
- Stern, J. H., J. M. Rutkowski, and P. E. Scherer. 2016. Adiponectin, leptin, and fatty acids in the maintenance of metabolic homeostasis through adipose tissue crosstalk. *Cell Metab.* **23**: 770–784.
- Smith, U., and B. B. Kahn. 2016. Adipose tissue regulates insulin sensitivity: role of adipogenesis, de novo lipogenesis and novel lipids. *J. Intern. Med.* **280**: 465–475.
- Tandon, P., R. Wafer, and J. E. N. Minchin. 2018. Adipose morphology and metabolic disease. *J. Exp. Biol.* **221**: doi:10.1242/jeb.164970.
- Cariou, B., K. van Harmelen, D. Duran-Sandoval, T. H. van Dijk, A. Grefhorst, M. Abdelkarim, S. Caron, G. Torpier, J. C. Fruchart, F. J. Gonzalez, et al. 2006. The farnesoid X receptor modulates adiposity and peripheral insulin sensitivity in mice. *J. Biol. Chem.* **281**: 11039–11049.
- Rizzo, G., M. Disante, A. Mencarelli, B. Renga, A. Gioiello, R. Pellicciari, and S. Fiorucci. 2006. The farnesoid X receptor promotes adipocyte differentiation and regulates adipose cell function in vivo. *Mol. Pharmacol.* **70**: 1164–1173.
- Abdelkarim, M., S. Caron, C. Duhem, J. Prawitt, J. Dumont, A. Lucas, E. Bouchaert, O. Briand, J. Brozek, F. Kuipers, et al. 2010. The farnesoid X receptor regulates adipocyte differentiation and function by promoting peroxisome proliferator-activated receptor-   and interfering with the Wnt/beta-catenin pathways. *J. Biol. Chem.* **285**: 36759–36767.
- Prawitt, J., M. Abdelkarim, J. H. Stroeve, I. Popescu, H. Duez, V. R. Velagapudi, J. Dumont, E. Bouchaert, T. H. van Dijk, A. Lucas, et al. 2011. Farnesoid X receptor deficiency improves glucose homeostasis in mouse models of obesity. *Diabetes*. **60**: 1861–1871.
- Horton, J. D., I. Shimomura, S. Ikemoto, Y. Bashmakov, and R. E. Hammer. 2003. Overexpression of sterol regulatory element-binding protein-1a in mouse adipose tissue produces adipocyte hypertrophy, increased fatty acid secretion, and fatty liver. *J. Biol. Chem.* **278**: 36652–36660.
- Kassam, A., B. Miao, P. R. Young, and R. Mukherjee. 2003. Retinoid X receptor (RXR) agonist-induced antagonism of farnesoid X receptor FXR activity due to absence of coactivator recruitment and decreased DNA binding. *J. Biol. Chem.* **278**: 10028–10032.
- Werner, A., D. M. Minich, R. Havinga, V. Bloks, H. van Goor, F. Kuipers, and H. J. Verkade. 2002. Fat malabsorption in essential fatty acid-deficient mice is not due to impaired bile formation. *Am. J. Physiol. Gastrointest. Liver Physiol.* **283**: G900–G908.
- Jung, H. R., S. M. Turner, R. A. Neese, S. G. Young, and M. K. Hellerstein. 1999. Metabolic adaptations to dietary fat malabsorption in chylomicron-deficient mice. *Biochem. J.* **343**: 473–478.
- Oosterveer, M. H., T. H. van Dijk, U. J. Tietge, T. Boer, R. Havinga, F. Stellaard, A. K. Groen, F. Kuipers, and D. J. Reijngoud. 2009. High fat feeding induces hepatic fatty acid elongation in mice. *PLoS One*. **4**: e6066.
- Bligh, E. G., and W. J. Dyer. 1959. A rapid method of total lipid extraction and purification. *Can. J. Biochem. Physiol.* **37**: 911–917.
- van Dijk, T. H., A. J. Laskewitz, A. Grefhorst, T. S. Boer, V. W. Bloks, F. Kuipers, A. K. Groen, and D. J. Reijngoud. 2013. A novel approach to monitor glucose metabolism using stable isotopically labelled glucose in longitudinal studies in mice. *Lab. Anim.* **47**: 79–88.

35. Alnouti, Y., I. L. Csanaky, and C. D. Klaassen. 2008. Quantitative-profiling of bile acids and their conjugates in mouse liver, bile, plasma, and urine using LC-MS/MS. *J. Chromatogr. B Analyt. Technol. Biomed. Life Sci.* **873**: 209–217.
36. Lin, K., H. Kools, P. J. de Groot, A. K. Gavai, R. K. Basnet, F. Cheng, J. Wu, X. Wang, A. Lommen, G. J. Hooiveld, et al. 2011. MADMAX - management and analysis database for multiple ~omics experiments. *J. Integr. Bioinform.* **8**: 160.
37. Dennis, G., Jr., B. T. Sherman, D. A. Hosack, J. Yang, W. Gao, H. C. Lane, and R. A. Lempicki. 2003. DAVID: Database for Annotation, Visualization, and Integrated Discovery. *Genome Biol.* **4**: P3.
38. Subramanian, A., P. Tamayo, V. K. Mootha, S. Mukherjee, B. L. Ebert, M. A. Gillette, A. Paulovich, S. L. Pomeroy, T. R. Golub, E. S. Lander, et al. 2005. Gene set enrichment analysis: a knowledge-based approach for interpreting genome-wide expression profiles. *Proc. Natl. Acad. Sci. USA.* **102**: 15545–15550.
39. Alvarez-Llamas, G., E. Szalowska, M. P. de Vries, D. Weening, K. Landman, A. Hoek, B. H. Wolffenbuttel, H. Roelofsen, and R. J. Vonk. 2007. Characterization of the human visceral adipose tissue secretome. *Mol. Cell. Proteomics.* **6**: 589–600.
40. Roelofsen, H., M. Dijkstra, D. Weening, M. P. de Vries, A. Hoek, and R. J. Vonk. 2009. Comparison of isotope-labeled amino acid incorporation rates (CILAIR) provides a quantitative method to study tissue secretomes. *Mol. Cell. Proteomics.* **8**: 316–324.
41. Cariou, B., K. van Harmelen, D. Duran-Sandoval, T. van Dijk, A. Grefhorst, E. Bouchaert, J. C. Fruchart, F. J. Gonzalez, F. Kuipers, and B. Staels. 2005. Transient impairment of the adaptive response to fasting in FXR-deficient mice. *FEBS Lett.* **579**: 4076–4080.
42. Duran-Sandoval, D., B. Cariou, F. Percevault, N. Hennuyer, A. Grefhorst, T. H. van Dijk, F. J. Gonzalez, J. C. Fruchart, F. Kuipers, and B. Staels. 2005. The farnesoid X receptor modulates hepatic carbohydrate metabolism during the fasting-refeeding transition. *J. Biol. Chem.* **280**: 29971–29979.
43. Wang, Q. A., C. Tao, R. K. Gupta, and P. E. Scherer. 2013. Tracking adipogenesis during white adipose tissue development, expansion and regeneration. *Nat. Med.* **19**: 1338–1344.
44. Halberg, N., T. Khan, M. E. Trujillo, I. Wernstedt-Asterholm, A. D. Attie, S. Sherwani, Z. V. Wang, S. Landskroner-Eiger, S. Dineen, U. J. Magalang, et al. 2009. Hypoxia-inducible factor 1 α induces fibrosis and insulin resistance in white adipose tissue. *Mol. Cell. Biol.* **29**: 4467–4483.
45. Wernstedt Asterholm, I., and P. E. Scherer. 2016. Fibrosis-streaks and splatters: Some things are not always what they seem to be. *Obesity (Silver Spring)*. **24**: 552–553.
46. Swift, J., I. L. Ivanovska, A. Buxboim, T. Harada, P. C. Dingal, J. Pinter, J. D. Pajeroski, K. R. Spinler, J. W. Shin, M. Tewari, et al. 2013. Nuclear lamin-A scales with tissue stiffness and enhances matrix-directed differentiation. *Science*. **341**: 1240104.
47. Perry, R. J., J. P. Camporez, R. Kursawe, P. M. Titchenell, D. Zhang, C. J. Perry, M. J. Jurczak, A. Abudukadier, M. S. Han, X. M. Zhang, et al. 2015. Hepatic acetyl CoA links tissue inflammation to hepatic insulin resistance and type 2 diabetes. *Cell*. **160**: 745–758.
48. Hellerstein, M. K., and R. A. Neese. 1992. Mass isotopomer distribution analysis: a technique for measuring biosynthesis and turnover of polymers. *Am. J. Physiol.* **263**: E988–E1001.
49. Sinal, C. J., M. Tohkin, M. Miyata, J. M. Ward, G. Lambert, and F. J. Gonzalez. 2000. Targeted disruption of the nuclear receptor FXR/BAR impairs bile acid and lipid homeostasis. *Cell*. **102**: 731–744.
50. Kok, T., C. V. Hulzebos, H. Wolters, R. Havinga, L. B. Agellon, F. Stellaard, B. Shan, M. Schwarz, and F. Kuipers. 2003. Enterohepatic circulation of bile salts in farnesoid X receptor-deficient mice: efficient intestinal bile salt absorption in the absence of ileal bile acid-binding protein. *J. Biol. Chem.* **278**: 41930–41937.
51. Samuel, V. T., and G. I. Shulman. 2016. The pathogenesis of insulin resistance: integrating signaling pathways and substrate flux. *J. Clin. Invest.* **126**: 12–22.
52. Rosen, E. D., and B. M. Spiegelman. 2014. What we talk about when we talk about fat. *Cell*. **156**: 20–44.
53. Wang, Q. A., C. Tao, L. Jiang, M. Shao, R. Ye, Y. Zhu, R. Gordillo, A. Ali, Y. Lian, W. L. Holland, et al. 2015. Distinct regulatory mechanisms governing embryonic versus adult adipocyte maturation. *Nat. Cell Biol.* **17**: 1099–1111.
54. Faust, I. M., P. R. Johnson, J. S. Stern, and J. Hirsch. 1978. Diet-induced adipocyte number increase in adult rats: a new model of obesity. *Am. J. Physiol.* **235**: E279–E286.
55. Watanabe, M., Y. Horai, S. M. Houten, K. Morimoto, T. Sugizaki, E. Arita, C. Matak, H. Sato, Y. Tanigawara, K. Schoonjans, et al. 2011. Lowering bile acid pool size with a synthetic farnesoid X receptor (FXR) agonist induces obesity and diabetes through reduced energy expenditure. *J. Biol. Chem.* **286**: 26913–26920.
56. Kim, S. M., M. Lun, M. Wang, S. E. Senyo, C. Guillermier, P. Patwari, and M. L. Steinhauser. 2014. Loss of white adipose hyperplastic potential is associated with enhanced susceptibility to insulin resistance. *Cell Metab.* **20**: 1049–1058.
57. Guillermier, C., P. K. Fazeli, S. Kim, M. Lun, J. P. Zuflacht, J. Milian, H. Lee, H. Francois-Saint-Cyr, F. Horreard, D. Larson, et al. 2017. Imaging mass spectrometry demonstrates age-related decline in human adipose plasticity. *JCI Insight*. **2**: e90349.
58. Cariou, B., E. Bouchaert, M. Abdelkarim, J. Dumont, S. Caron, J. C. Fruchart, R. Burcelin, F. Kuipers, and B. Staels. 2007. FXR-deficiency confers increased susceptibility to torpor. *FEBS Lett.* **581**: 5191–5198.
59. Seale, P., S. Kajimura, W. Yang, S. Chin, L. M. Rohas, M. Uldry, G. Tavernier, D. Langin, and B. M. Spiegelman. 2007. Transcriptional control of brown fat determination by PRDM16. *Cell Metab.* **6**: 38–54.
60. Suchy, F. J., W. F. Balistreri, J. E. Heubi, J. E. Searcy, and R. S. Levin. 1981. Physiologic cholestasis: elevation of the primary serum bile acid concentrations in normal infants. *Gastroenterology*. **80**: 1037–1041.
61. Wen, J. H., L. G. Vincent, A. Fuhrmann, Y. S. Choi, K. C. Hribar, H. Taylor-Weiner, S. Chen, and A. J. Engler. 2014. Interplay of matrix stiffness and protein tethering in stem cell differentiation. *Nat. Mater.* **13**: 979–987.
62. Gjorevski, N., N. Sachs, A. Manfrin, S. Giger, M. E. Bragina, P. Ordóñez-Morán, H. Clevers, and M. P. Lutolf. 2016. Designer matrices for intestinal stem cell and organoid culture. *Nature*. **539**: 560–564.
63. Mariman, E. C. M., and P. Wang. 2010. Adipocyte extracellular matrix composition, dynamics and role in obesity. *Cell. Mol. Life Sci.* **67**: 1277–1292.
64. Marcelin, G., A. Ferreira, Y. Liu, M. Atlan, J. Aron-Wisnewsky, V. Pelloux, Y. Botbol, M. Ambrosini, M. Fradet, C. Rouault, et al. 2017. A PDGFR α -mediated switch toward CD9^{high} adipocyte progenitors controls obesity-induced adipose tissue fibrosis. *Cell Metab.* **25**: 673–685.
65. Sun, C., W. L. Berry, and L. E. Olson. 2017. PDGFR α controls the balance of stromal and adipogenic cells during adipose tissue organogenesis. *Development*. **144**: 83–94.
66. Shao, M., L. Vishvanath, N. C. Busbuso, C. Hepler, B. Shan, A. X. Sharma, S. Chen, X. Yu, Y. A. An, Y. Zhu, et al. 2018. De novo adipocyte differentiation from Pdgfr β ⁺ preadipocytes protects against pathologic visceral adipose expansion in obesity. *Nat. Commun.* **9**: 890.
67. Vigouroux, C., A. C. Guénant, C. Vatiér, E. Capel, C. Le Dour, P. Afonso, G. Bidault, V. Béréziat, O. Lascos, J. Capeau, et al. 2018. Lipodystrophic syndromes due to LMNA mutations: recent developments on biomolecular aspects, pathophysiological hypotheses and therapeutic perspectives. *Nucleus*. **9**: 235–248.
68. Wernstedt Asterholm, I., C. Tao, T. S. Morley, Q. A. Wang, F. Delgado-Lopez, Z. V. Wang, and P. E. Scherer. 2014. Adipocyte inflammation is essential for healthy adipose tissue expansion and remodeling. *Cell Metab.* **20**: 103–118.
69. Lee, K. Y., S. J. Russell, S. Ussar, J. Boucher, C. Vernochet, M. A. Mori, G. Smyth, M. Rourk, C. Cederquist, E. D. Rosen, et al. 2013. Lessons on conditional gene targeting in mouse adipose tissue. *Diabetes*. **62**: 864–874.
70. Donnelly, K. L., C. I. Smith, S. J. Schwarzenberg, J. Jessurun, M. D. Boldt, and E. J. Parks. 2005. Sources of fatty acids stored in liver and secreted via lipoproteins in patients with nonalcoholic fatty liver disease. *J. Clin. Invest.* **115**: 1343–1351.
71. Hijmans, B. S., C. A. Tiemann, A. Grefhorst, M. Boesjes, T. H. van Dijk, U. J. Tietge, F. Kuipers, N. A. van Riel, A. K. Groen, and M. H. Oosterveer. 2015. A systems biology approach reveals the physiological origin of hepatic steatosis induced by liver X receptor activation. *FASEB J.* **29**: 1153–1164.